Research Division of Materials Joining Process, Dep. of Energy Control of Processing

Journal of Physics D: Applied Physics, 51, (2017), 015204 (14pp).
doi:10.1088/1361-6463/aa9902

Experimental Investigation on Weld Pool Formation Process in Plasma Keyhole Arc Welding

Nguyen Van Anh*, Shinichi Tashiro**, Bui Van Hanh***, Manabu Tanaka****

Abstract (159Words)

This paper seeks to clarify weld pool formation process in PKAW. We adopted, for the first time, measurement of three-dimensional convection inside the weld pool in PKAW using X-ray transmission systems. Two-dimensional convection on weld pool surface was also measured using zirconia tracer particles. To discuss heat transport process in the weld pool, two-dimensional temperature distribution on the weld pool surface was also measured by the two-color pyrometry. The results indicate that the shear force due to plasma flow is found to be the dominant driving force in weld pool formation process in PKAW. Thus, the heat transport in the weld pool is considered to be governed by two large convective patterns near keyhole. They are formed with equal velocity of approximately 0.35 m/s and are mainly driven by shear force. Furthermore, the flow velocity of weld pool convection becomes considerably higher than that of other welding process such as GTAW and GMAW due to larger plasma flow velocity.

Keywords

Plasma keyhole arc welding; Weld pool formation process; X-ray observation; Flow velocity measurement; Temperature measurement

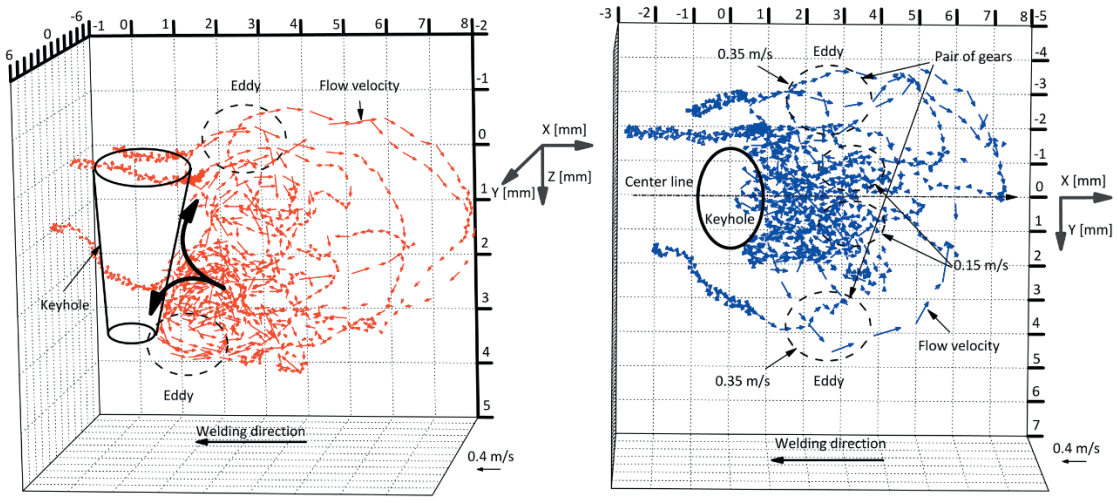

(a) perspective view (b) top view

Fig.1.

Three-dimensional convective patterns inside weld pool.

* Graduate School Student
** Assistant Professor
*** Hanoi University of Science and Technology
**** Professor

Journal of Applied Physics, 122 (2017) 033301
doi: 10.1063/1.4993715

Development of a Non-equilibrium 60 MHz Plasma Jet with a Long Discharge Plume

Giichiro Uchida*, Kazufumi Kawabata**, Taiki Ito**, Kosuke Takenaka***, Yuichi Setsuhara****

Abstract(182words)

High-frequency plasma jets driven by voltages in the frequency range 6–60 MHz are developed. A long plasma jet 40 mm in length is successfully produced by using a pair of ring electrodes outside a quartz tube. The electrode pair consists of a wide power electrode and a narrow ground electrode that is positioned at the head of the tube. The ratio of the length of the ground electrode to the length of the power electrode must be small in order to produce the long plasma jets. The high-frequency plasma jet is operated in a non-thermal-equilibrium state at a gas temperature of around 60 °C. Operation at the very-high-frequency of 60 MHz leads to a lower discharge voltage and lower electron energy compared with the lower frequencies of 6 and 13.56 MHz. The ability of the very-high-frequency 60 MHz plasma jet to produce reactive oxygen and nitrogen species in water is also investigated. High H_2O_2 and NO_3^- concentrations of more than 1 mmol/l are realized by irradiating 3 ml of deionized water with the plasma for the short period of 2 min.

Keywords

Nonthermal plasma jet; High density plasma source; Reactive oxygen and nitrogen species

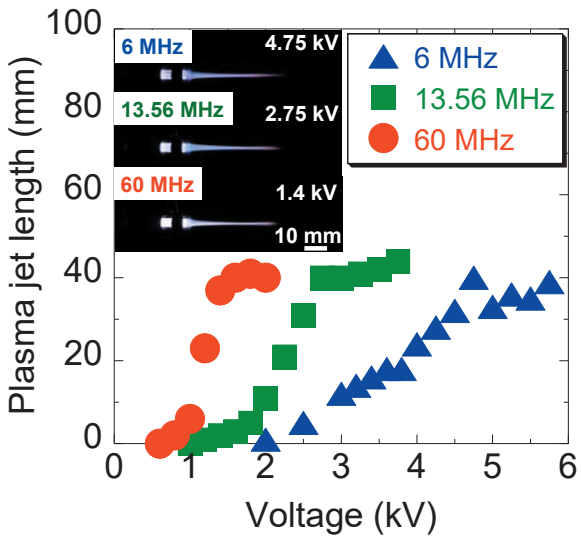

Fig.1
Dependence of the plasma-jet length on the applied peak-to-peak voltage for driving-voltage frequencies of 6, 13.56, and 60 MHz. The Ar gas flow rate was 3 slm. The photographs show high-frequency plasma jets 40 mm in length for driving-voltage frequencies of 6, 13.56, and 60 MHz. Reproduced from Journal of Applied Physics, 122, 033301 (2017), with the permission of AIP Publishing.

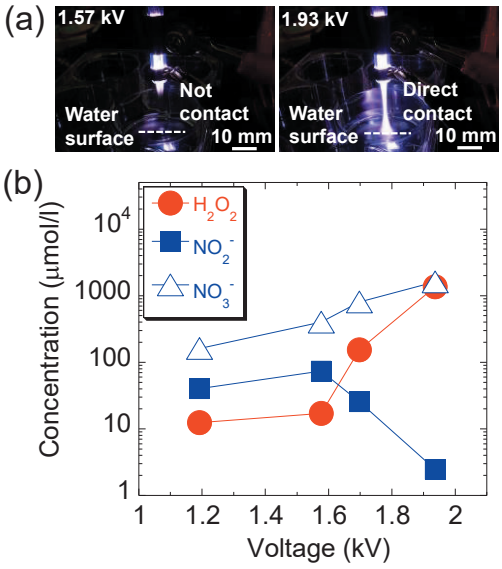

Fig.2
(a) Photographs deionized water being irradiated by the VHF plasma jet (60 MHz). (b) Dependence of H_2O_2, NO_2^-, and NO_3^- concentrations in the plasma-irradiated water on the applied peak-to-peak voltage. The 60 MHz plasma jet was used to irradiate 3 ml of deionized water for 2 min. Reproduced from Journal of Applied Physics, 122, 033301 (2017), with the permission of AIP Publishing.

* Associate Professor
** Graduate School Student
*** Assistant Professor
**** Professor

Optics & Laser Technology,99,(2017),326-332
https://doi.org/10.1016/j.optlastec.2017.09.019

Suppression of Dilution in Ni-Cr-Si-B Alloy Cladding Layer by Controlling Diode Laser Beam Profile

Daichi Tanigawa*, Yoshinori Funada**, Nobuyuki Abe***, Masahiro Tsukamoto****, Yoshihiko Hayashi*****, Hiroyuki Yamazaki******, Yoshihiro Tasumi*******, Mikio Yoneyama*******

Abstract (148 Words)

A Ni-Cr-Si-B alloy layer was produced on a type 304 stainless steel plate by laser cladding. In order to produce cladding layer with smooth surface and low dilution, influence of laser beam profile on cladding layer was investigated. A laser beam with a constant spatial intensity at the focus spot was used to suppress droplet formation during the cladding layer formation. This line spot, formed with a focussing unit designed by our group, suppressed droplet generation. The layer formed using this line spot with a constant spatial intensity had a much smoother surface compared to a layer formed using a line spot with a Gaussian-like beam. In addition, the dilution of the former layer was much smaller. These results indicated that a line spot with a constant spatial intensity was more effective in producing a cladding layer with smooth surface and low dilution because it suppressed droplet generation.

Keywords

Laser cladding, Flat-top profile, Diode laser, Surface roughness, Dilution

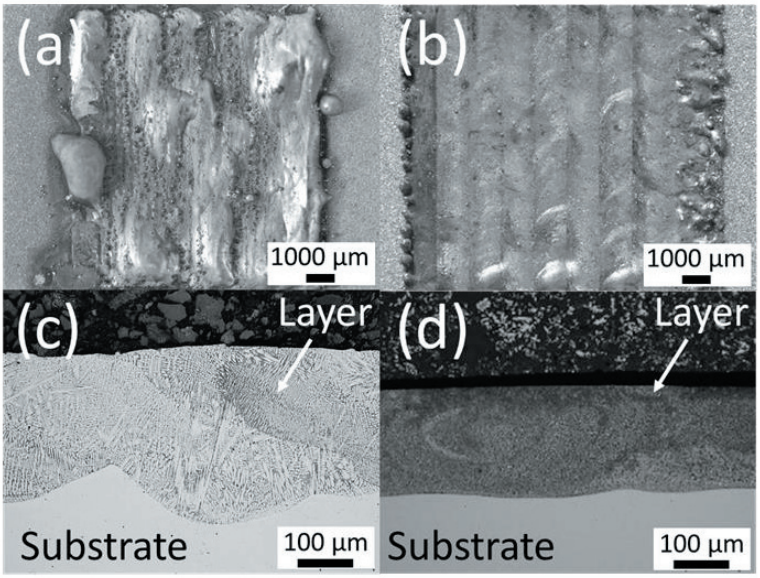

Fig.. Optical images of the cladding layer surfaces formed with (a) a Gaussian-like beam and (b) a flat-top beam. Cross-sections of the cladding layers in (a) and (b) are shown in (c) and (d), respectively

* Graduate School Student
** Industrial Research Institute of Ishikawa
*** Specially Appointed Professor
**** Professor
***** Specially Appointed Assistant Professor
****** Specially Appointed Associate Professor
******* Osaka Fuji Corporation

Journal of Manufacturing Processes, 26, (2017), 122–130.
doi:10.1016/j.jmapro.2017.02.007

A New Process for Design and Manufacture of Tailor-made Functionally Graded Composites through Friction Stir Additive Manufacturing

Abhay Sharma*, Bandari Vijendra*, Kazuhiro Ito**, Kazuyuki Kohama***, M. Ramji*, B.V. Himasekhar Sai*

Abstract (195Words)

Motivated by the recent use of friction stirring in the manufacture of in-situ composites, a new additive manufacturing method for the design and manufacture of tailor-made functionally graded composites is presented.

The existing literature on the subject matter is limited to creating functional grades in the vicinity of the weld nugget without direct control on composition and property gradients. A mathematical model is developed for achieving a compositional gradient over a predefined length in a metal matrix composite and subsequently demonstrated through the manufacture of aluminum+TiC functionally graded composite. Progressive gradients are observed in hardness and local mechanical properties, namely, Young's modulus, strain hardening exponent, and yield stress obtained using the digital image correlation technique. The process mechanism is elucidated by correlating results of mechanical tests and electron backscatter diffraction analysis. A specific process condition vis-à-vis the number of passes, volume fraction, and particle size combination may promote one or more phenomena such as continuous dynamic recrystallization, particle fragmentation, and breaking of initial matrix grains, which eventually affect particle mixing and matrix grain size and thus cause property gradients. The findings are expected to enable the manufacture of functionally graded composites products of larger size.

Keywords

Functionally graded composite; Friction stirring; Additive manufacturing; Mechanical properties; Microstructural analysis; Digital image correlation

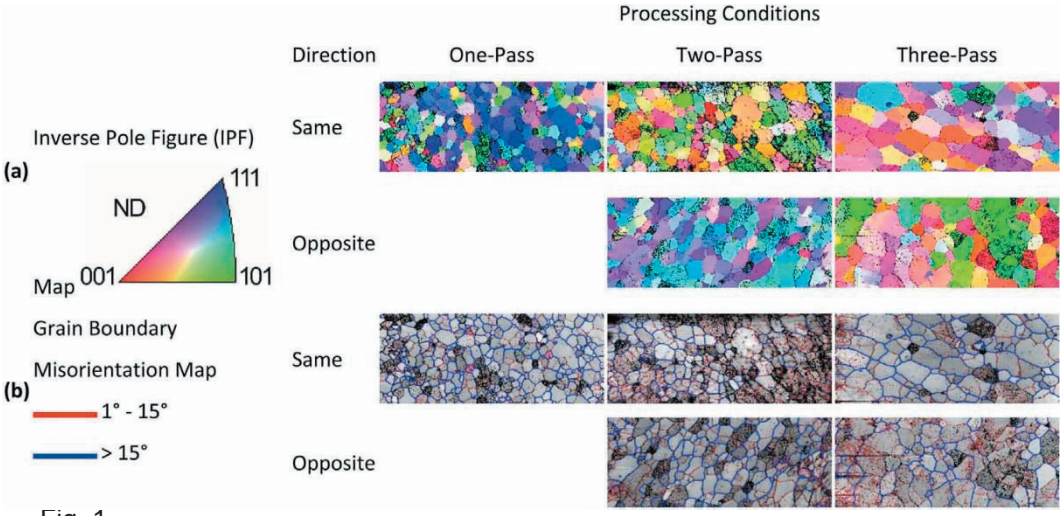

Fig. 1.
Inverse pole figures and grain boundary misorientation maps.

* Indian Institute of Technology Hyderabad
** Professor
*** Assistant Professor

Research Division of Materials Joining Mechanism, Dep. of Joint Interface Structure and Formation Mechanism

Materials and Design, 129, (2017), 151–163.
http://dx.doi.org/10.1016/j.matdes.2017.05.013

Clarification of Microstructure Evolution of Aluminum during Friction Stir Welding using Liquid CO_2 Rapid Cooling

Xiaochao Liu*, Yufeng Sun**, Hidetoshi Fujii***

Abstract

The microstructure evolution of aluminum during friction stir welding was reconstructed using tool "stop action" technique. Simultaneous liquid CO_2 was used to "freeze" the weld microstructure and the transient microstructure after "stop action". Subsequent short-time annealing produced a situation similar to the normal cooling. The microstructure evolution during the deformation and annealing stages was investigated along the material flow and in the "frozen" weld zone, respectively, by high-resolution electron-backscatter-diffraction technique. The results showed that the base material evolved into microstructures containing large amount of low angle grain boundaries (44.8%) with strong (7.9 times) $B/\overline{B}$ shear texture at the initial welding stage. With the increasing of welding strain, lamellar grain structure with strong (6.1 times) $A/\overline{A}$ shear texture was developed. Next, continuous dynamic recrystallization via lattice rotation with the grain <101> orientation as the rotation axis occurred under the strain relaxation condition, leading to lamellar grains conversion into equiaxed grains. Meanwhile, the strong $A/\overline{A}$ texture transformed into weak (2.9 times) β-fiber textures (dominated by $B/\overline{B}$ and C components). At the cooling stage, preferred grain growth along {112}<110> occurred, forming relatively strong (3.8 times) $B/\overline{B}$ texture.

Keywords

Friction stir welding; Rapid cooling; Annealing; Microstructure evolution; Grain structure; Texture

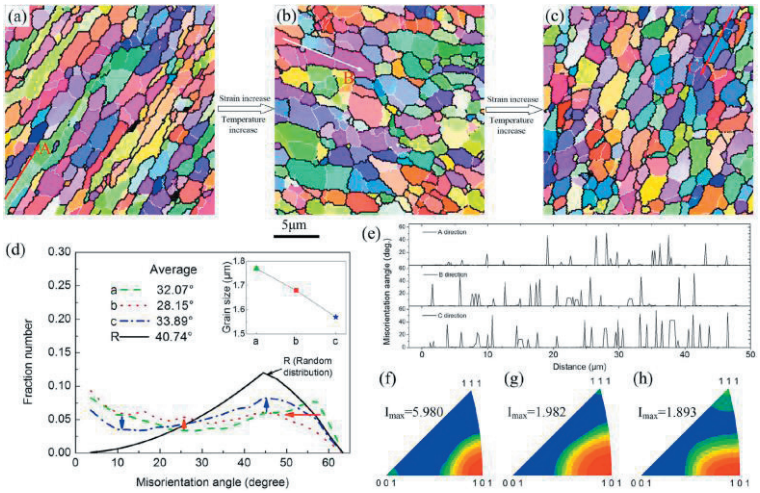

Fig. 1. Grain structure development from LS to TS: (a–c) are the inverse pole figure maps; (d) the misorientation angle distributions and average grain size of a, b and c; (e) misorientation distributions measured along the grain elongation directions; (f–h) are the inverse pole figures of the grains in a, b and c for their respective shear directions.

* Graduate school student
** Specially appointed associate professor
*** Professor

Acta Materialia 140 (2017), 317-325.
doi.org/10.1016/j.actamat.2017.08.048

Length Effect of Carbon Nanotubes on the Strengthening Mechanisms in Metal Matrix Composites

Biao Chen*, Jianghua Shen*, Lei Jia**, Shufeng Li**, Junko Umeda***, Makoto Takahashi****, Katsuyoshi Kondoh*****

Abstract (145 Words)

In the present work, we studied the effect of the aspect ratio of carbon nanotubes (CNTs) on strengthening aluminum metal matrix composites (Al MMCs). To this end, Al samples reinforced with CNTs of various aspect ratios were produced via three different powder metallurgy methods. Microstructural examination revealed that the CNTs were uniformly dispersed in the materials with a range of aspect ratios from 6.5 to 55. The tensile results showed that the CNTs exhibited a strong strengthening effect in the composites regardless of their aspect ratios. However, the post-loading examination and quantitative analysis indicated that there was a strengthening mechanism transition for CNTs, which was closely associated with the aspect ratio or length of CNTs. The origin of such transition was explored from the viewpoint of dislocation-CNTs interaction under loading. The findings may provide a new insight in understanding the strengthening behaviors of CNT-reinforced MMCs.

Keywords

Metal matrix composite; Carbon nanotubes; Strengthening Mechanism; Load transfer; Length effect; Orowan mechanism

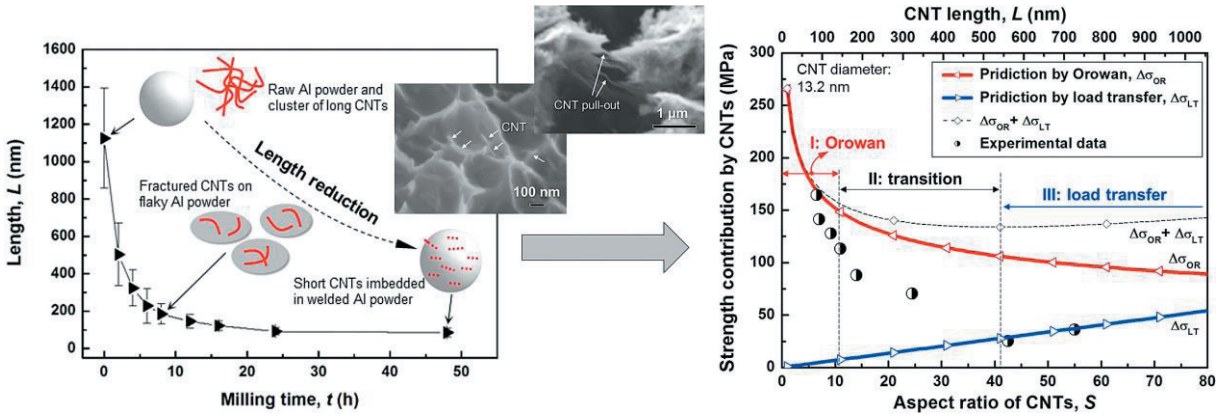

Fig. 1 Length changes of un-bundled CNTs on Al powder surface by mechanical milling and dependence of strength contribution by CNTs on aspect ratio or length of CNTs dispersed in Al matrix composites fabricated by powder metallurgy route.

* Specially Appointed Researcher
** Professor, Xi'an University of Technology
*** Associate Professor
**** Lecture
***** Professor

Journal of Materials Processing Technology, 243 (2017) 387–394.
doi:10.1016/j.jmatprotec.2016.12.021

Measurement of Residual Stress in Arc Welded Lap Joints by cosα X-ray Diffraction Method

Jian Lina*, Ninshu Ma**, Yongping Lei*, Hidekazu Murakawa**

Abstract (144Words)

The welding residual stress of lap joints of thin steel sheets was measured by the cosα X-ray diffraction method and compared with the numerical simulation. The longitudinal residual stress in the region near the weld is close to the yield strength of the base metal. The welding residual stress distribution is asymmetrical on the two plates and two sides of the weld because of the asymmetrical geometry of the lap joint. A higher residual stress was observed on the lower plate of lap joints. The longitudinal residual stress has almost the uniform distribution along the weld line except near two ends. The influencing length near two ends of the weld line is about 20–30 mm. The maximum tensile value of the longitudinal residual stress of the lap joint of the high strength steel TS590 is higher than that of the mild steel TS270.

Keywords: Residual stress, X-ray diffraction measurement method, Lap joints, Arc welding, Numerical simulation

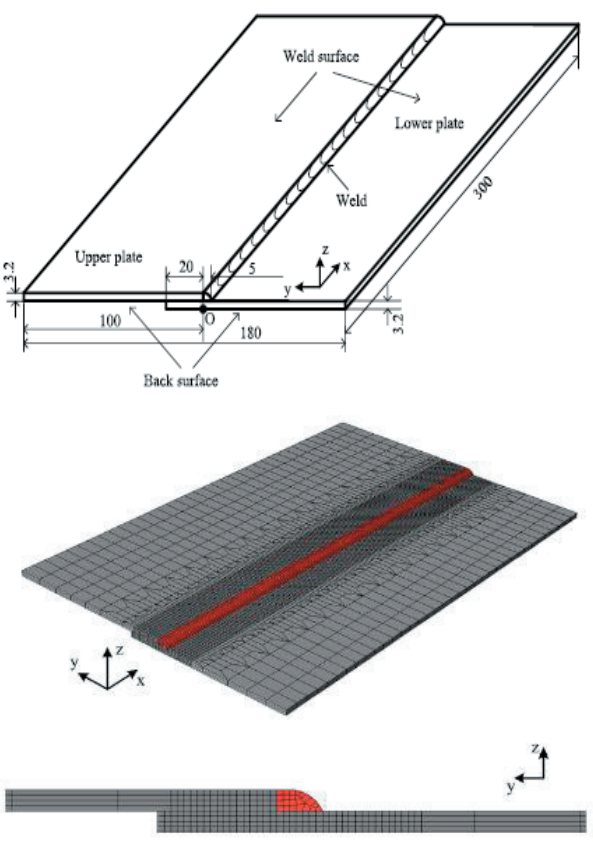

Fig. 1. Finite element model of arc welded lap joint.

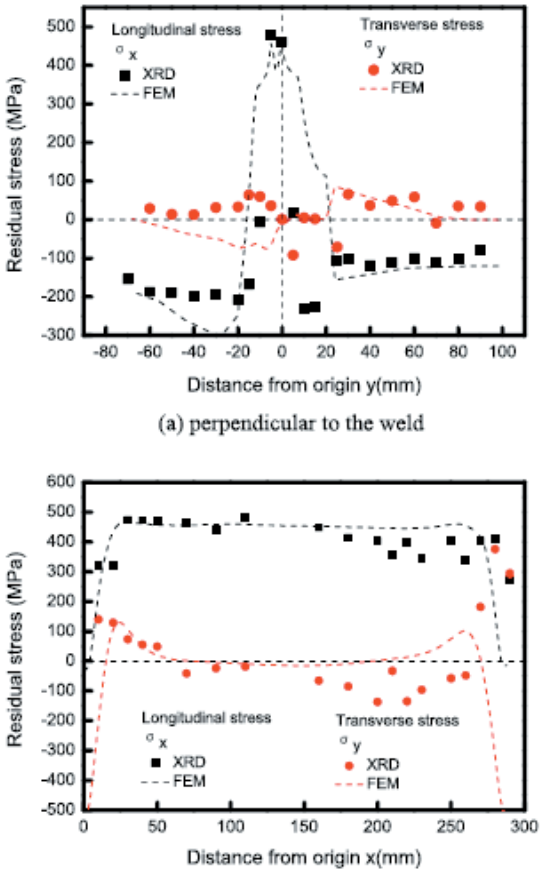

Fig. 2. Comparison of the computed and measured welding residual stress.

* Beijing University of Technology
** Professor, Osaka University

Research Division of Materials Joining Assessment, Dep. of Structural Integrity and Failure Assessment

Theoretical and Applied Fracture Mechanics, 92, (2017), 178–184.
doi:10.1016/j.tafmec.2017.07.013

Observation of Micro-cracks beneath Fracture Surface during Dynamic Crack Propagation

Yasuhito Takashima*, Tomoya Kawabata**, Suguru Yamada***, Fumiyoshi Minami****

Abstract (200Words)

In this study, micro-cracks generated during dynamic crack propagation were investigated for an ESSO specimen and V-notched Charpy specimen. The ESSO test with temperature gradient and the Charpy impact test were conducted for steel for shipbuilding. The macroscopic roughness of the fracture surface increases with increasing temperature. The section beneath the fracture surface generated during dynamic brittle crack propagation was observed using a scanning electron microscope, after cutting with a focused ion beam or grinding. Many micro-cracks can be found beneath the brittle fracture surface in the V-notched Charpy specimen. In the ESSO specimen, which had a macroscopic flat surface, micro-cracks can be detected beneath the main crack propagated in the temperature range from –140°C to –100°C. On the other hand, there were a few micro-cracks beneath the main crack propagated at relatively high temperature, at which the fracture surface was macroscopically rough. The number of micro-cracks in the Charpy specimen is fewer than those in the ESSO specimen at the same temperature. The observations indicated that the correlations of Charpy impact properties with crack arrest performance for the ESSO specimen was inconvincible in terms of the differences in the micro-scale fracture behavior as well as lack of theoretical basis.

Keywords

Notched specimen; Brittle fracture; Rapid crack propagation; Cleavage micro-crack; Structural steel

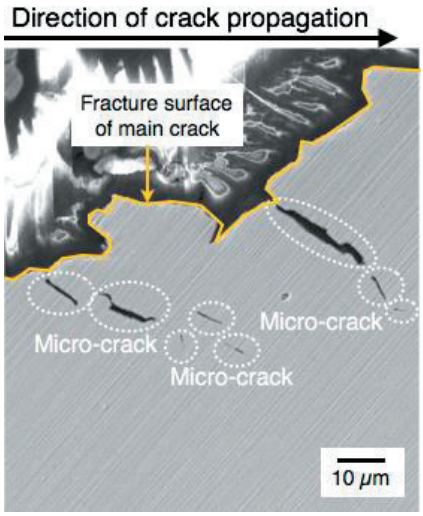

Fig. 1.
Micro-cracks observed beneath the fracture surface in Charpy and ESSO specimens.

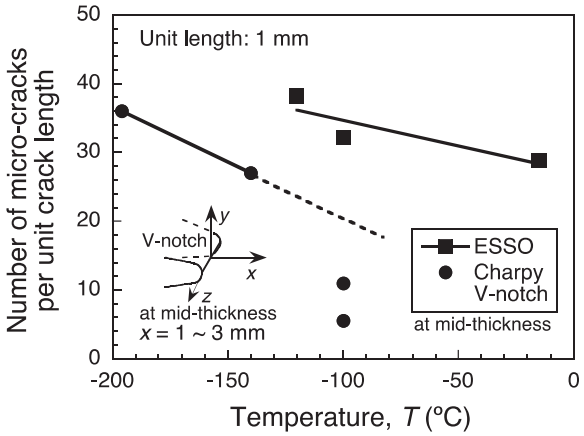

Fig. 2.
Temperature dependence of number of micro-cracks beneath the fracture surface generated during dynamic brittle crack propagation.

* Assistant Professor
** University of Tokyo
*** Graduate School Student
**** Professor

Acta Mechanica , 228, (2017), 4213–4233.
doi: 10.1007/s00707-017-1926-0

Closest-point Projection Method for the Extended Subloading Surface Model

Riccardo Fincato*, Seiichiro Tsutsumi**

Abstract (111Words)

This paper presents the implementation of a fully implicit integration scheme (i.e. closest-point projection method) of an unconventional plasticity model, the Extended Subloading Surface Model. The aim is to obtain precise solutions for elastoplastic investigations of metals subjected to cyclic loading, even for large prescribed loading conditions. A previous incomplete implicit integration scheme (i.e. cutting-plane method) for the model was already formulated. However, this study offers an alternative form, which increase the accuracy of the similarity center variable. The numerical Finite Element Analyses (FEA) show local and global quadratic convergence rates, proving the correct implementation of the integration scheme. Moreover, iso-error maps were computed to show the accuracy of the algorithm.

Keywords

Fatigue; Numerical techniques; Return mapping; Extended Subloading Surface; Cyclic plasticity.

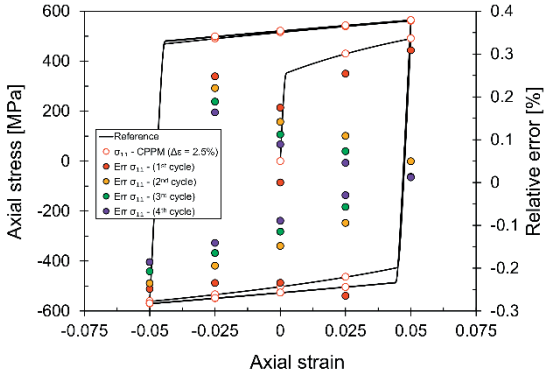

Fig. 1.
Axial stress vs axial strain and relative errors per cycle for a cubic element under uniaxial cyclic loading.

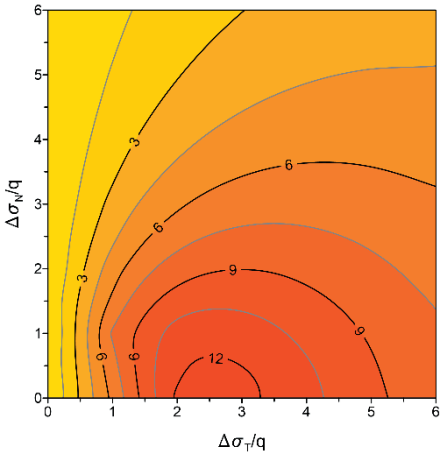

Fig. 2.
Iso-error map for the stress, purely biaxial initial condition.

* Specially Appointed Assistant Professor
** Associate Professor

Research Division of Materials Joining Assessment, Dep. of Reliability Evaluation &Simulation

Metallurgical and Materials Transactions A, 48, (2017), 5860-5869
doi: 10.1007/s11661-017-4340-2

Effect of Chemical Composition on Susceptibility to Weld Solidification Cracking in Austenitic Weld Metal

Kota Kadoi*, Kenji Shinozaki **

Abstract (146Words)

The influence of the chemical composition, especially the niobium content, chromium equivalent Cr_{eq}, and nickel equivalent Ni_{eq}, on the weld solidification cracking susceptibility in the austenite single-phase region in the Schaeffler diagram was investigated. The distributions of the susceptibility (crack length and BTR) in the diagram revealed a region with high susceptibility to solidification cracking. Addition of niobium enhanced the susceptibility and changed the distribution of the susceptibility in the diagram. The BTR distribution was in good agreement with the distribution of solidification temperature range (ΔT) calculated by solidification simulation. ΔT increased with increasing content of alloying elements such as niobium. The distribution of ΔT was dependent on the type of alloying element owing to the change of the partitioning behavior. The distribution of the susceptibility in the region is controlled by the change in ΔT and the segregation behavior of niobium with the chemical composition.

Keywords

Solidification cracking susceptibility, Austenitic metal, Dissimilar weld metal, Dilution ratio, Schaeffler diagram, Stainless steel

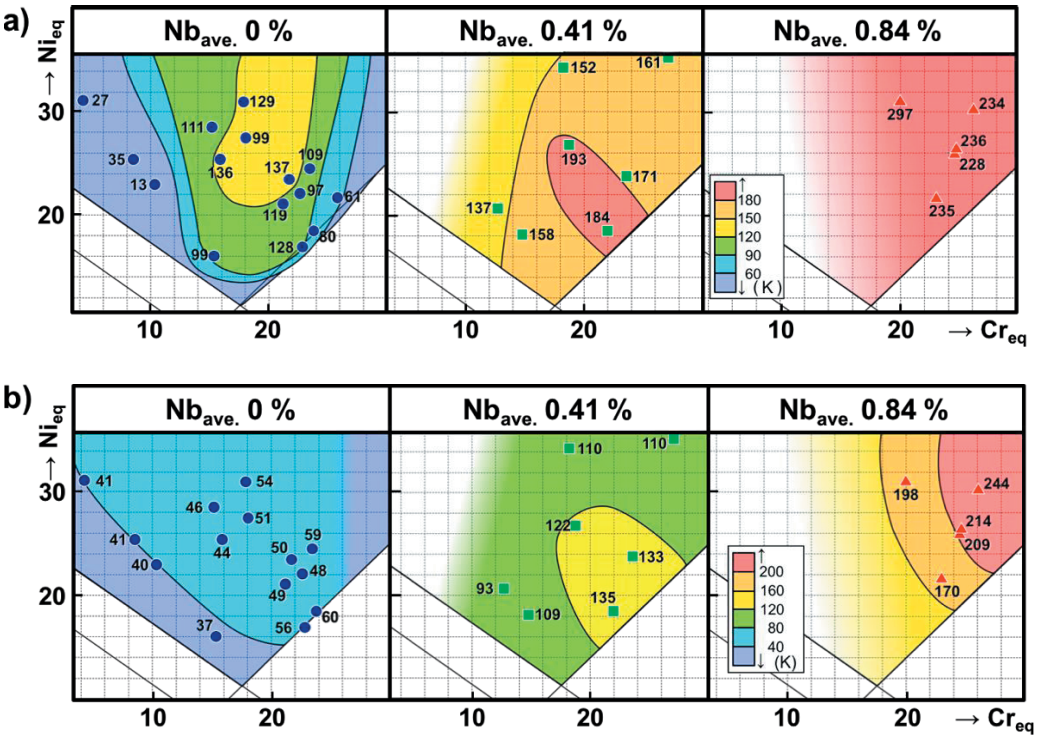

Fig.
Distributions of BTR and ΔT in Schaeffler diagram. a) BTR. b) ΔT.

* Associate Professor
** Hiroshima University

Advanced Powder Technology, 28 (2017) 50-54.
10.1016/j.apt.2016.07.017

Effect of BaF_2 Powder Addition on the Synthesis of YAG Phosphor by Mechanical Method

Kazuaki Kanai*, Yoshifumi Fukui*, Takahiro Kozawa**, Akira Kondo***, Makio Naito****

Abstract (93 Words)

Here, we report on the effect of BaF_2 powder addition on the mechanical synthesis of Ce^{3+}-doped $Y_3Al_5O_{12}$ ($Y_{2.97}Al_5O_{12}:Ce_{0.03}^{3+}$, YAG:$Ce^{3+}$) phosphors for white light emitting diodes. The YAG phosphors were synthesized by the mechanical method using an attrition-type mill. When BaF_2 was added at 6 wt% to the raw powder materials and milled, the synthesis of YAG:Ce^{3+} was favorably achieved at the vessel temperature of 255 °C, which was about 1200 °C lower than the YAG phosphor synthesis temperature by solid-state reaction. The synthesized YAG:Ce^{3+} phosphor revealed the maximum internal quantum yield of 57%.

Keywords

YAG:Ce^{3+}; Phosphor; White light emitting diode; Attrition-type mill; Mechanical synthesis; BaF_2

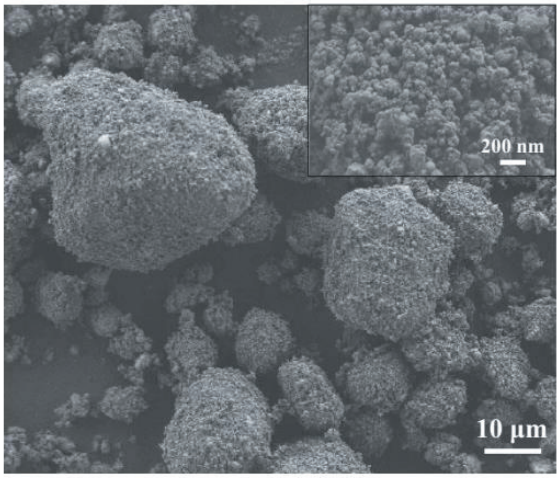

Fig.1. SEM image of sample B.

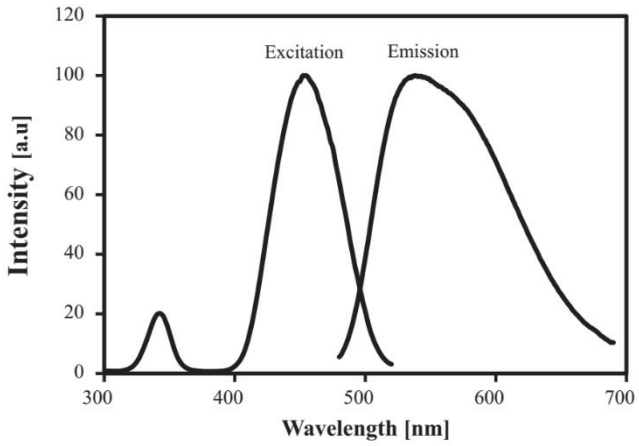

Fig.2. Excitation and emission spectra of YAG phosphor of sample B.

* Kaneka Corporation
** Assistant Professor
*** Specially Appointed Researcher
**** Professor

Ceramic Interconnect and Ceramic Microsystems Technology, 13, 1, (2017), 225-231

Ultraviolet Laser Stereolithography of Alumina Lattice with a Diamond Pattern

Soshu Kirihara*

Abstract (141Words)

In additive manufacturing of ultraviolet lithography, 2D cross sections were created through dewaxing and sintering by high power laser drawing on spread resin paste including ceramic nanoparticles, and 3D composite models were sterically printed by layer lamination and micro joining. The lithographic system has been developed to obtain bulky ceramic components with functional geometries. As the row material of the lithography, nanometer sized ceramic particles were dispersed in to liquid resins at 50 % in volume fraction. The resin paste was spread on a glass substrate at 100 μm in layer thickness by a mechanically moved knife edge. The ultraviolet laser beam of 355 nm in wavelength was adjusted at 50 μm in diameter and scanned on the pasted resin surface. The irradiation power was changed automatically from 1 to 10 W for enough dewaxing and sintering depth for layer bonding.

Keywords

Additive manufacturing; Ceramics; Stereolithography

Fig. An alumina micro lattice with a diamond type periodic pattern fabricated by using ultraviolet stereo -lithography. The ceramic component was formed from resin paste including nanoparticles through dewaxed and sintered by ultraviolet laser beam scanning.

* Professor

J Mater Sci: Mater Electron, 28 (2017), 12606-12616.
https://doi.org/10.1007/s10854-017-7085-1

Thermal Stability of Low-temperature Sintered Joint using Sn-coated Cu Particles during Isothermal Aging at 250 °C

Xiangdong Liu*, Shiqi Zhou*, Hiroshi Nishikawa**

Abstract (125Words)

We investigate the microstructural stability of a Cu–Cu joint sintered with microscale Cu particles and Sn-coated Cu (Cu@Sn) particles during an isothermal aging. Using Cu particles and Cu@Sn particles as die attach materials, pure Cu discs were bonded at 200 °C for 20 min with an applied pressure of 10 MPa in a formic acid atmosphere. Then, the isothermal aging test was conducted at 250 °C in an air atmosphere. The Cu@Sn sintered joints showed much better thermal stability than the Cu sintered joint. The joint presented nearly 20 MPa shear strength after the aging for 1000 h. The Cu_3Sn IMC network suppressed the oxidation of Cu both in the sintered layer and on the substrate, thereby maintaining the microstructural integrity of the Cu@Sn sintered joint.

Keywords

Pb-free high temperature bonding, Sn-coated Cu particle, Thermal stability, Shear strength

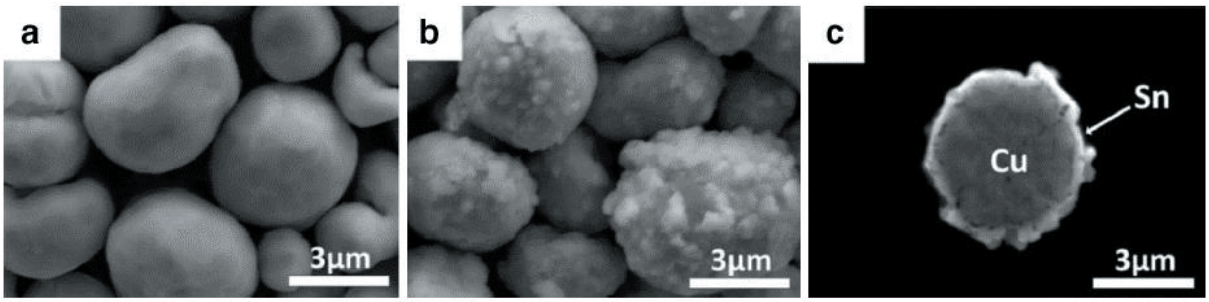

Fig. 1 Typical SEM images of the microscale particles used in this study: a Cu particles, b Sn-coated Cu particles, and c cross section of a Sn-coated Cu particle.

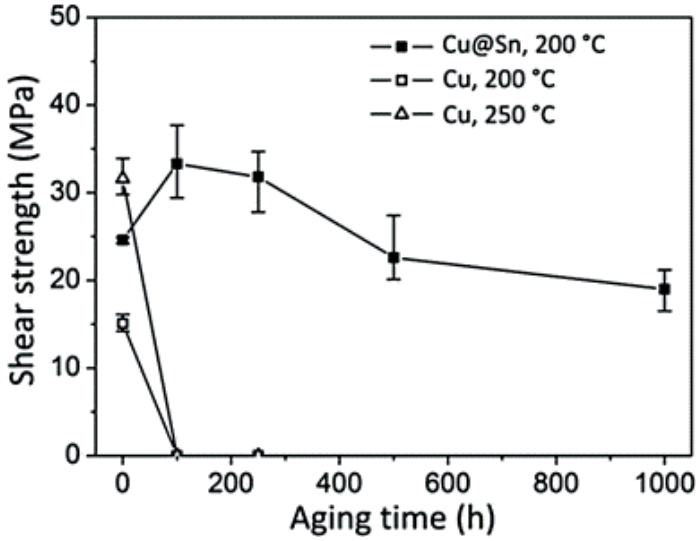

Fig. 2 Variation of the shear strength of the Cu@Sn joints and the Cu joints during the isothermal aging test at 250 °C.

* Graduate School Student
** Associate Professor

Journal of the European Ceramic Society, 37, (2017) 5339-5345.
doi.org/10.1016/j.jeurceramsoc.2017.05.056

Spherical Porous Granules in MgO-Fe_2O_3-Nb_2O_5 System: *In situ* Observation of Formation Behavior using High-temperature Confocal Laser-scanning Microscopy

Yoshikazu Suzuki*, Hiroya Abe****, Hajime Yamamoto***, Kazuhiro Ito*****, Hiroshige Inoue*****, Mayumi Nakamura**

Abstract (109Words)

The pyrolytic reactive granulation process, yielding ceramic spherical porous granules, is simple, consisting of typical ceramic processing methods, viz., wet-ball milling of powders, vacuum drying, granulation via sieving through a screen mesh, and one-step heat treatment for local reactive sintering within each granule. Here, the microstructural development of spherical porous granules was successfully visualized by in situ high-temperature confocal laser-scanning microscopy during the heating up to 1400 °C in air. Based on the result of the in situ observation, a simple but powerful size-controlling process of spherical porous granules, viz., multiscreen sieving after the heating was demonstrated. Nearly monodispersed spherical porous granules composed of pseudobrookite-type MgFeNbO5 were easily obtained.

Keywords

Spherical porous granule (SPG); *In situ* observation; Confocal laser-scanning microscopy (CLSM); Pseudobrookite; $MgFeNbO_5$

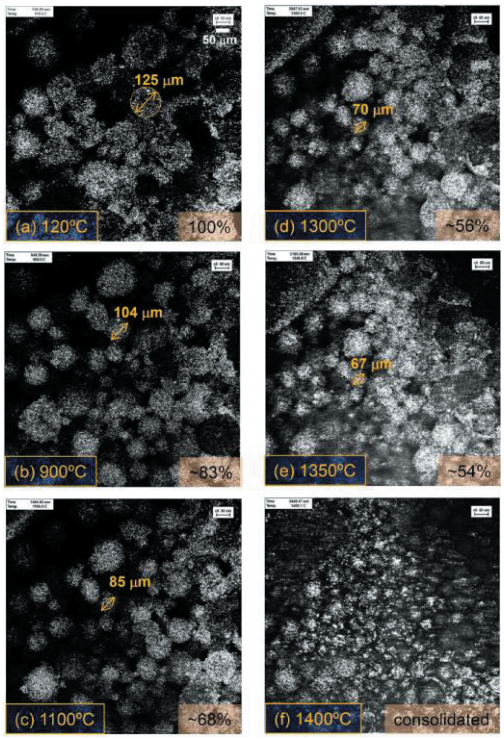

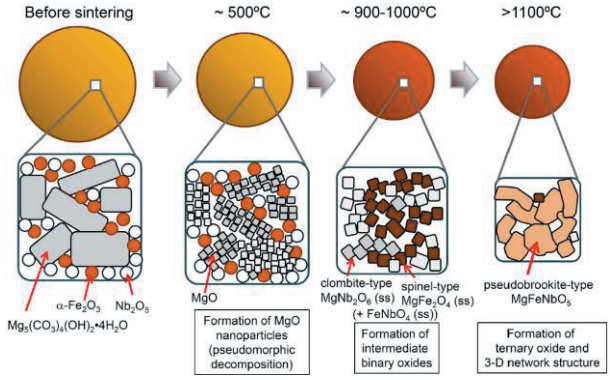

Fig.1 Microstructure development of sphere porous granules observed by in situ high-temperature confocal laser-scanning microscopy (left). Schematic illustration of the microstructure development during the heating (right).

* University of Tsukuba
** Yonekura MFG Co.
*** Graduate School Student
**** Associate Professor
***** Professor

溶接構造シンポジウム 2017 講演論文集, (2017), 189-192

Development of Bead Shape Measurement Technology for Pipe Welds

パイプ溶接部のビード形状計測技術の開発

Yohei ABE*, Mitsuyoshi NAKATANI **, Masahiko ADACHI ***, Kazuhiko TANI ***, Hisato YUTO***

阿部　洋平，中谷 光良，足達　昌彦，谷　和彦，湯藤　尚人

Abstract (103 Words)

The strength of pipe welds is assured by the throat thickness. The required throat thickness varies according to the angle between pipes, which varies at different positions. It is difficult to measure the throat thickness of the pipe welds by visual testing or using a weld gauge. We have developed the bead shape measurement equipment for pipe welds. The equipment collects two-dimensional point data on the bead shape of a weld using an optical cutting method, determines the leg length and throat thickness by data processing and makes a pass/fail judgment against the required values at the measuring point.

Keywords

Inspection technique/ Bead shape measurement/ Optical cutting method/ Pipe welds

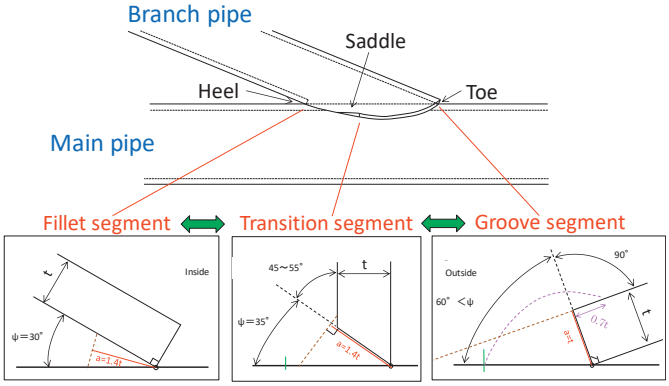

Fig.1 Groove shape of pipe welds.

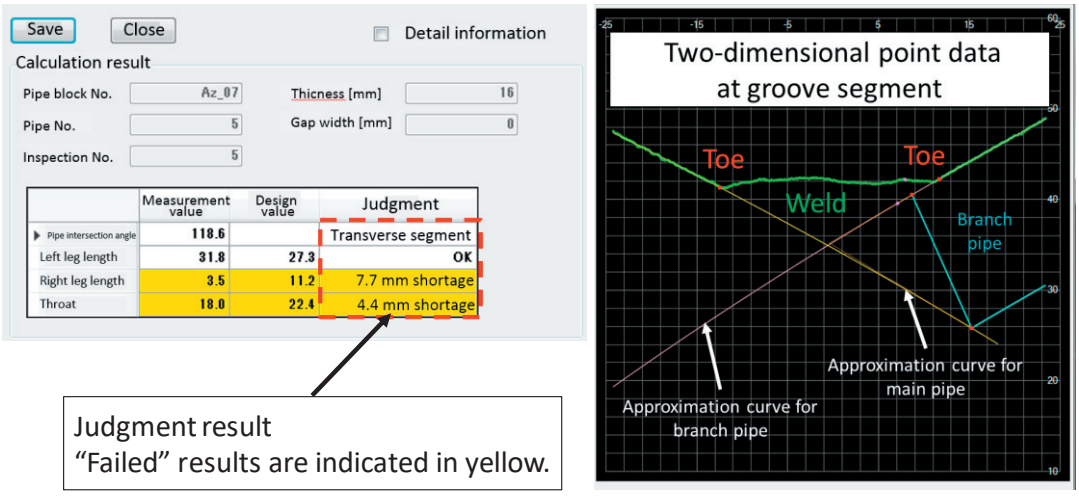

Fig.2 Measurement result screen.

*　Specially Appointed Assistant Professor
**　Specially Appointed Associate Professor
***　Hitachi Zosen Corporation

Special Budget Project of the Ministry of Education, Culture, Sports, Science and Technology, Development Base on Creation of Life Innovation Materials for Interdisciplinary and International Researcher Development

International Journal of Hydrogen Energy, 42, (2017), 9493-9499.
Doi: 10.1149/2.1191613jes

Effects of NiO-loading on n-type GaN Photoanode for Photoelectrochemical Water Splitting using Different Aqueous Electrolyte

Kayo Koike*, Kazuhiro Yamamoto**, Satoshi Ohara***, Tomoka Kiritsu****, Kazunari Ozasa****, Shinichiro Nakamura****, Masakazu Sugiyama*, Yoshiaki Nakano*, Katsushi Fujii*

Abstract (165Words)

n-type GaN photoanodes used for water splitting have stability problems. One means of resolving this is loading NiO catalyst on the n-type GaN surface. Aqueous electrolytes H_2SO_4, HCl, KOH, and NaOH are usually used for photoelectrochemical water splitting. However, suitable electrolytes for the NiO-loading on n-type GaN photoelectrode have not yet been evaluated. Therefore, we investigated the effects of changing electrolytes used for NiO-loading in this study. The photocurrent of NiO-loading on n-type GaN increased when KOH and NaOH electrolytes were used. In addition, the surfaces showed no corrosion after reaction when these electrolytes were used. However, the photocurrent was not stable using KOH electrolyte. Interestingly, stable photocurrent was observed with when the NaOH electrolyte was used. In the case of H_2SO_4, the photocurrent of GaN did not change with and without NiO. The surface morphologies became rough because of GaN corrosion, and NiO dissolved in the H_2SO_4 electrolyte.

Keywords

GaN; Photoanode; Water splitting; Anodic corrosion; NiO

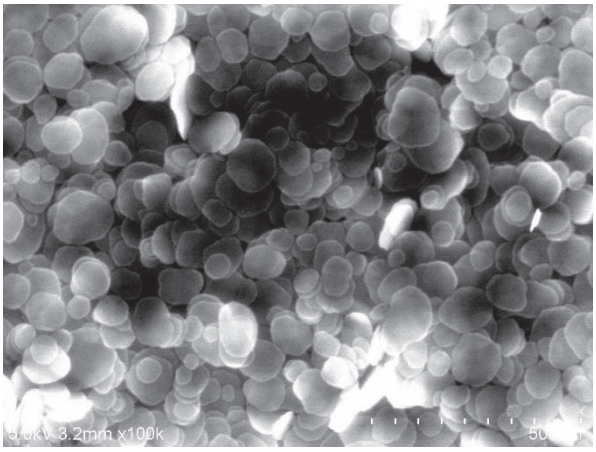

Fig. 1. NiO precursor nanoparticles synthesized at Joining and Welding Research Institute, Osaka University.

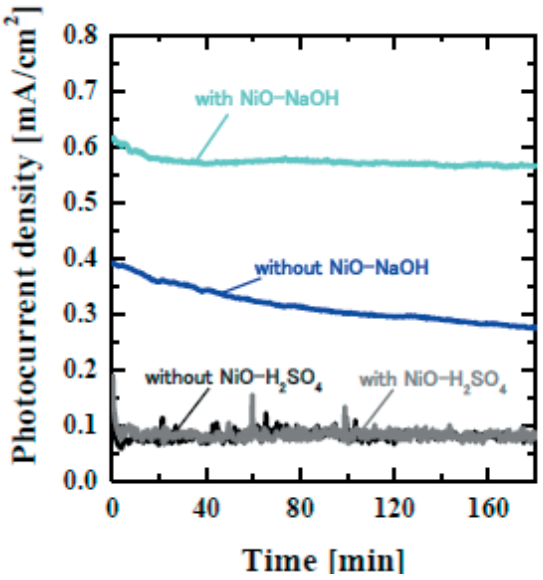

Fig. 2. The time variation of the photocurrent density with and without NiO using 0.5M H_2SO_4 and 1.0M NaOH electrolytes.

* The University of Tokyo
** NIMS
*** Specially Appointed Professor
**** RIKEN

Activity Report on "The Project to Create Research and Educational Hubs for Innovative Manufacturing in Asia"

Mihoko KATSUMATA*, Futoshi HIMI **, Yosuke KAWAHITO ***

Abstract (206Words)

In this project, the three pillars were set; 1) Establish a global network of researchers in joining technologies across Greater Asia Region, 2) Develop new key technologies for joining adaptable to extreme environments, 3) Implement oversea internships which tie up students from area of science and the humanities, named as Coupling internships (CIS). Results of this year's activities were reported as below.

1) Total of 8 international joint researches including 2 newly commenced and 6 continuous researches from previous years were implemented. 2 workshops with National Taiwan University, Thailand National Metal and Material Technology Center, and one International Symposium with the invited domestic and oversea speakers were organized. Through the Joint Researches shown in Table 1, 34 international joint papers were posted.
2) Research on Underwater Laser Welding Technology was in the final stage to examine its quality of underwater welding process as well as underwater cutting with invented torch and robot.
3) Coupling Internship was conducted in 5 countries; Indonesia, Vietnam, Thailand, India, and Singapore. Pictures from CIS can be found in Fig. 1 and Fig. 2.
4) Based on the networks, JWRI received 17 students in total from partner universities in Taiwan, Thailand, India, Vietnam, Malaysia, Myanmar and Indonesia under JST Sakura Science Plan.

Table 1 List of International Joint Research in 2017

Partner University	Research Topics
King Mongkut's University of Technology, Thonburi (Thailand)	Advanced high-strength titanium powder metallurgy materials for medical devices
Indian Institute of Technology, Hyderabad (India)	Relationship between structure and cooling rate of three-dimensional modeling using arc welding
National Metal and Materials Technology Center (Thailand)	Stereolithographic additive manufacturing of biomaterials implants
Indian Institute of Technology, Hyderabad (India)	Relationship between mechanical properties and microstructure of welds in Twin-wire GMAW welding of low carbon steel
Nanyang Technological University (Singapore)	Residual stress modeling and fatigue life prediction in laser cladding specimen
Indian Institute of Technology, Hyderabad (India)	Research on the melting phenomenon in waveform-controlled SAW
National Metal and Materials Technology Center (Thailand)	Laser welding of titanium and CFRP
National Metal and Materials Technology Center (Thailand)	Strengthening effect of 316L stainless steel composite via Selective Laser Melting

Fig. 1 CIS Singapore

Fig. 2 CIS India

* Specially Appointed Associate Professor
** Specially Appointed Researcher
*** Associate Professor

Science and Technology of Welding and Joining, (2017) 1-6.

Resistance Spot Welding of Metal/carbon-fiber-reinforced Plastics and Applying Silane Coupling Treatment

Kimiaki NAGATSUKA*, Bolyu XIAO**, Lihui WU**, Kazuhiro NAKATA***, Shuhei SAEKI****, Yamato KITAMOTO**** and Yoshiaki IWAMOTO****

Abstract

Dissimilar materials joining of SUS304 and carbon-fiber-reinforced plastics consisting of short fibers and thermoplastics was performed. The materials were joined by series resistance spot welding. The electrodes were pressed on the metal plate of the lap joint of metal/carbon-fiber-reinforced plastics. The SUS304 plate was heated by resistance heating, causing the thermoplastic near the interface to melt slightly because of heat conduction. SUS304 could be joined directly to carbon-fiber-reinforced polyamide and modified polypropylene, but not to polyphenylene sulphide. The joining area increased with an increase in the welding current and welding time, so did the tensile shear fracture load. Furthermore, the silane coupling agent treatment of SUS304 was highly effective in increasing the joining strength.

KEYWORDS: Series resistance spot welding/ carbon-fiber-reinforced thermoplastic/ polyamide 6/ polypropylene/ polyphenylene sulphide/ stainless steel/ dissimilar materials joining/ silane coupling

* Specially Appointed Assistant Professor
** Specially Appointed Researcher
*** Specially Appointed Professor
**** DENGENSHA TOA CO., LTD

The ASME Journal of Electronic Packaging, 139, 4 (2017) 041010–1-13
doi: 10.1115/1.4038143

Solid-state Microjoining Mechanisms of Wire Bonding and Flip Chip Bonding

Yasuo TAKAHASHI*, Hiroki FUKUDA**, Yasuhiro YONESHIMA**, Hideki KITAMURA, Masakatsu. MAEDA***

Abstract

Trend of micro-joining is described. The microjoining within large scale integration (LSI) packages can be classified into three methods; wire bonding (WB), tape automated bonding (TAB), and flip chip bonding (FCB). In the present paper, Au wire (ball) bonding, FCB, Al wire bonding and Al ribbon bonding are discussed to understand the ultrasonic bonding mechanisms. Each type of microjoining takes on various aspects but has common bonding mechanisms regarding friction slip, plastic deformation, and friction heating. In the present paper, solid-state microjoining mechanisms in Au wire (ball) bonding, FCB, Al wire bonding, and Al ribbon bonding are discussed to systematically understand the common bonding mechanisms. Ultrasonic vibration enhances friction slip and plastic deformation, making it possible to rapidly obtain dry interconnects. Metallic adhesion at the central area of the bonding interface is mainly produced by the friction slip. On the other hand, the folding of the lateral side surfaces of the Au bump, Au ball, and Al wire is very important for increasing the bonded area. The central and peripheral adhesions are achieved by a slip-and-fold mechanism. The solid-state microjoining mechanisms are discussed based on experimental results. Fig. 1 shows scanning electron microscopic (SEM) photos of bonded top surfaces of Au bump for understanding the slip-and-fold-mechanism in FCB.

Keywords

Micro-joining; Electronics packaging; Low temperature; Wire bonding; Flip chip bonding; Ultrasonic; Al wire; Al ribbon

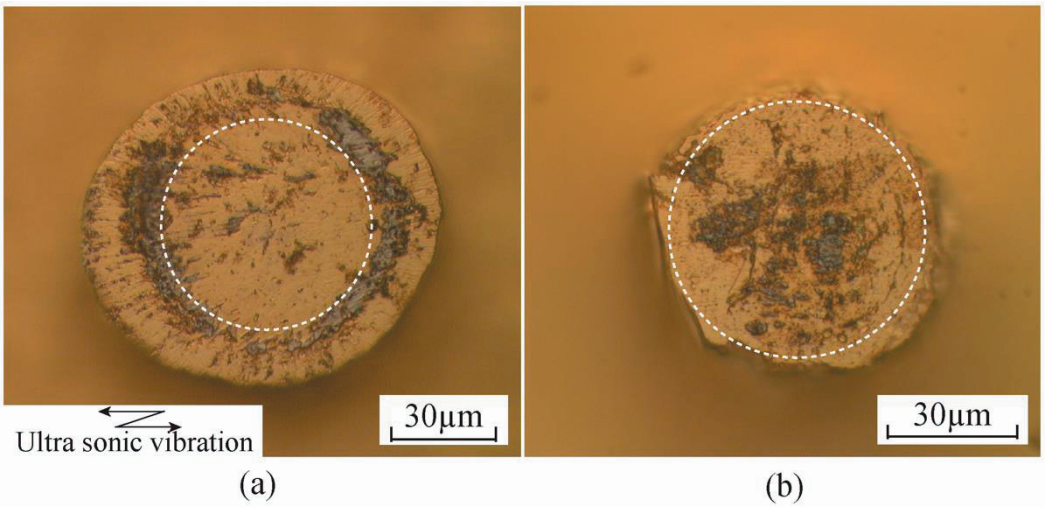

Fig. 1 SEM photos of the bonded top surfaces of Au bumps after etching the Al pads. Circles are drawn with white dotted lines. They express the diameter (~60μm) of the initial bonding surface (upper side of the bump). The blackish brown area is an alloy reaction phase. (a) high load and high ultrasonic power conditions (F = 1.0 N/bump, W_{US} = 300mW, t = 150ms). (b) low load and low ultrasonic power conditions (F = 0.43 N/bump, W_{US} = 50 mW, t = 100 ms).

* Specially Appointed Professor
** Graduate School Student
*** Nihon University

Quarterly J. Japan Welding Soc., 溶接学会論文集 35, 2 (2017), 47s-50s.

Study on Control of Cathode Spot Behavior in Arc Welding

Toshifumi Yuji*, Atsuhi Fujimaru*, Kentaro Yasui*, Hiroyuki Kinoshita*, Toshio Bouno**, Shinichi Tashiro***, Manabu Tanaka****

Abstract (135Words)

This study aims to clarify the mechanism of oxide layer removal process by cathode spots in AC TIG welding of aluminum plates and also to develop the technology to improve the oxide layer removal efficiency through the control of the cathode spot behavior. As a result of the observation of cathode spots with an ultra-high-speed video camera, it is found that the cathode spot velocity gradually increases with time during EP phase and reaches maximally 300 m/s. Furthermore, the average position of cathode spots is shifted toward the fringe of the weld pool in which the oxide layer still exists and arrives there around the end of EP phase. From this result, it is considered that the removal of the oxide layer by cathode spots is effectively performed only around the end of EP phase.

Keywords

AC TIG welding; Aluminum; Cathode spot, Oxide layer removal;

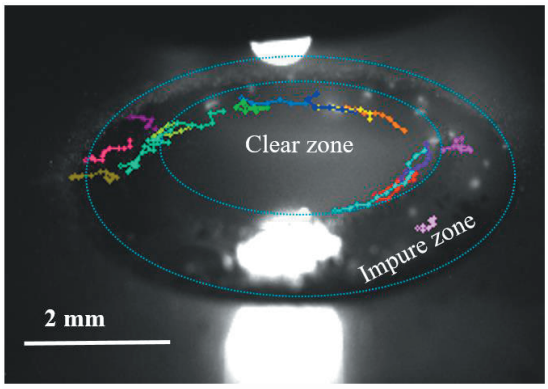

Fig.1.

Behavior of cathode spots around the end of EP phase observed with an ultra-high-speed video camera.

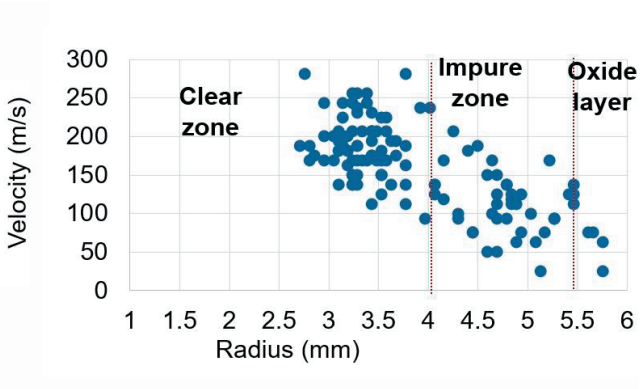

Fig.2.

Distribution of cathode spot velocity around the end of EP phase.

* Miyazaki University
** National Institute of Technology, Sasebo College
*** Assistant Professor
**** Professor

Applied Physics B-Lasers and Optics,119,(2015),545-549
https://doi.org/10.1007/s00340-015-6059-3

Surface Morphology of Ti-6Al-4V Plate Fabricated by Vacuum Selective Laser Melting

Y. Sato*, M. Tsukamoto**, Y. Yamashita***

Abstract (126 Words)

A plate made of Ti-6Al-4V (Ti64) was built by vacuum selective laser melting (SLM) at a pressure of 10-2 Pa. The vacuum SLM system employed a single mode fiber laser and three-axis galvanic mirror in order to form 3D metallic structure. In order to investigate the surface morphology on the fabricated plates, Vickers micro hardness and surface roughness Ra were measured. From the results, the Vickers micro hardness of the fabricated plates was recorded at 391 HV, higher than the typical 340 HV for a Ti64 plate. It was also determined that crystal orientation was evaluated with X-ray diffraction. From the results, the crystal orientation of powder is composed mainly of martensitic alpha. Diffraction peaks corresponding to β (110) were detected in vacuum SLM processed samples.

Keywords

Power Density Crystal Orientation, Additive Manufacturing, Molten Pool, Selective Laser Melting

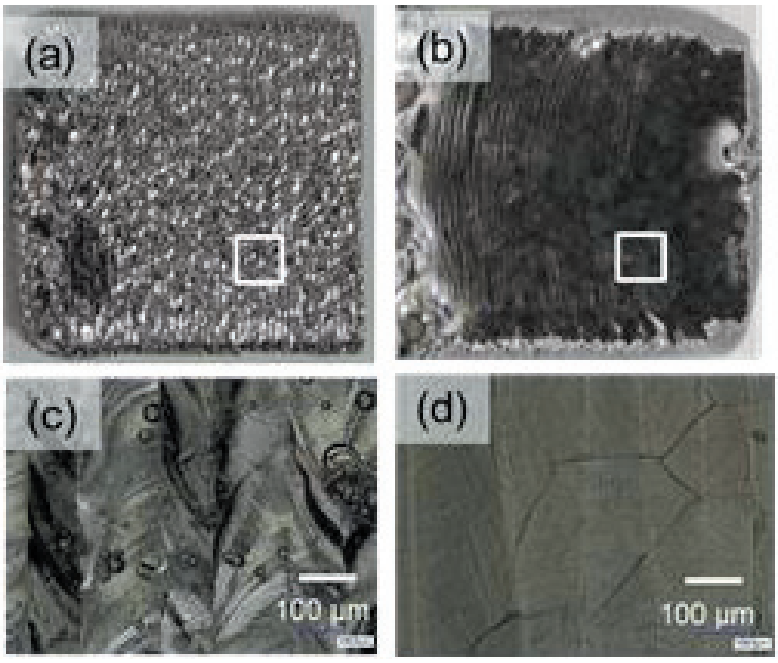

Fig. Optical images of the fabricated plate surfaces with a scanning speed of 50 mm/s and a hatching distance of 100 µm. Images (a) and (c) experienced a laser power density of 1.7×10^5 W/cm^2, while (b) and (d) had 1.1×10^6 W/cm^2. Images (c) and (d) are a higher magnification of (a) and (b), respectively.

* Specially Appointed Researcher
** Associate Professor
*** Industrial Research Institute of Ishikawa

Journal of light metal welding, 軽金属溶接 52, (2014), 453-462.
doi: https://doi.org/10.11283/jlwa.52.453

Dissimilar spot welding of three lapped sheets of aluminum alloy and steels by metal flow
-Application of Friction Anchor Welding to three lapped sheets of aluminum alloy and steels-

金属流動を利用したアルミニウム合金/鋼/鋼 3 枚重ね異種金属点接合
-摩擦アンカー接合のアルミニウム合金/鋼/鋼 3 枚重ね継手への適用-

Masaru SAKAMURA*, Kaoru OHISHI**, Kouhei OTA***, Yoshihiro TAKEYASU****, Shigeyuki MIZUNARI*****, Hidetoshi FUJII******
坂村勝，大石 郁，大田 耕平，竹保 義博，水成 重順，藤井 英俊

Abstract

A novel spot welding process for dissimilar metal lap joints using a new tool with the tip made of spherical ceramics, i.e., “Friction Anchor Welding,” was applied to three lapped sheets that consisted of an Al alloy (1.0-mm-thick A5052) and two steels (0.6-mm- and 1.0-mm-thick SPCC). Consequently, a steel projection was formed in the Al alloy sheet, and the sheets were welded at a plunge depth greater than 1.4 mm. The height of this steel projection increased with the plunge depth when the plunge depth was less than 2.2 mm; accordingly, the weld strength increased, and the tensile shear strength and the cross tensile strength reached approximately 3.8 kN/point and 2.5 kN/point, respectively. However, when the plunge depth was greater than 2.2 mm, the tip of the steel projection peeled off from the Al alloy, followed by cracks formation along the steel projection and the Al alloy interface, and the weld strength consequently decreased.

Keywords

Dissimilar metals, Metal flow, Projection, Three sheets, Steel, Aluminum alloy

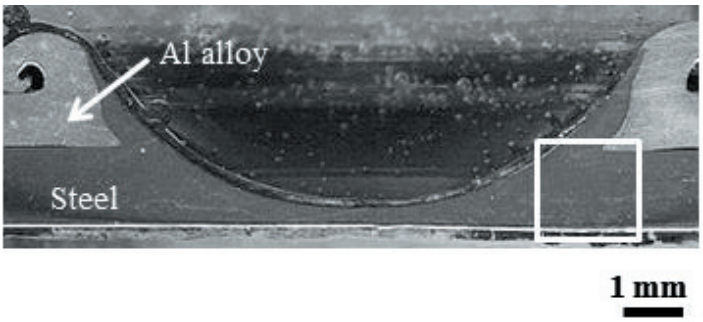

Fig. Cross-sectional macro image of the specimen (Pd: 2.2 mm).

* Hiroshima Prefectural Technology Research Institute
** Hiroshima Prefectural Technology Research Institute
*** Hiroshima Prefectural Technology Research Institute
**** Hiroshima Prefectural Technology Research Institute
***** Hiroshima Prefectural Technology Research Institute
****** Professor

Quarterly J. Japan Welding Soc., 35, 2 (2017) 165s-168s

Anisotropic Damage Constitutive Law for Cleavage Failure in Crystalline Grain by Cohesive Zone Model

Yuichi SHINTAKU*, Kenjiro TERADA**, Seiichiro TSUTSUMI***

Abstract (146Words)

The objective of this study is to propose new anisotropic damage constitutive law that represents the separation process on cleavage plane in a polycrystalline aggregate. The proposed law is formulated by embedding of the cohesive zone model (CZM) in a crystal plasticity constitutive law. The separation of the cleavage plane can be realized by exponential type of the CZM based on an atomic potential. On the other hands, the crystal plasticity constitutive law is used to simulate the deformation due to the crystalline slip on each crystallographic system. Thus, the proposed damage constitutive law is capable of representing the microscopic mechanism characterized by both the fracture behavior of the cleavage plane and the plastic deformation of the crystallographic slip. It is confirmed that the proposed model enables us to simulate the crack propagation in arbitrary directions, and the resultant anisotropic strength in a single crystal grain.

Keywords

Brittle fracture; Cleavage failure; Anisotropic damage; Crystal plasticity; Cohesive zone model

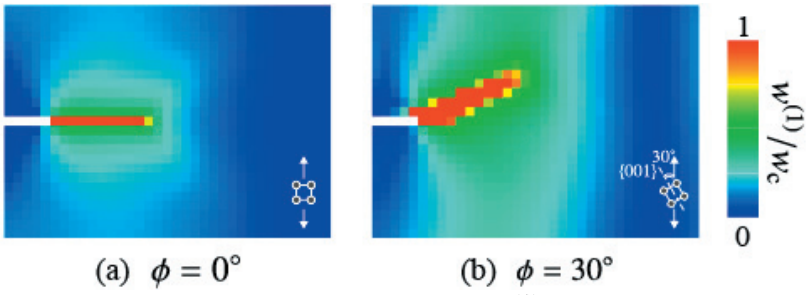

Fig. 1 Crack propagation with distribution of $w^{(1)}/w_c$ at final step.

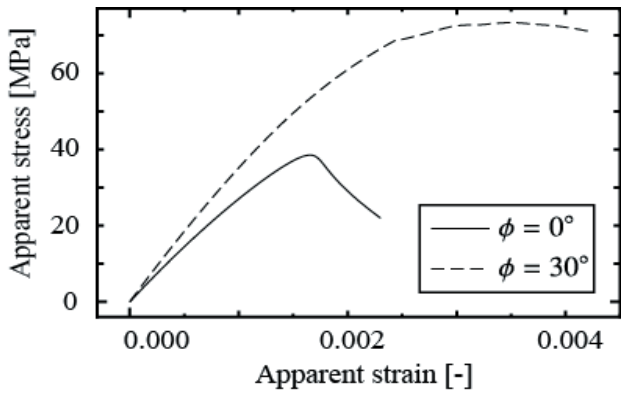

Fig. 2 Apparent stress-strain curve during crack propagation in single crystalline grain.

* Department of Engineering, University of Tsukuba
** International Research Institute of Disaster Science, Tohoku University
*** Associate Professor